Taylor & Francis
Taylor & Francis Group

Molecular Crystals and Liquid Crystals

ISSN: 1542-1406 (Print) 1563-5287 (Online) Journal homepage: http://www.tandfonline.com/loi/gmcl20

Formation of J-aggregates in Langmuir-Blodgett films: Effect of stearic acid and nano clay platelets

A. Shil, C. Debnath, S. A. Hussain & D. Bhattacharjee

To cite this article: A. Shil, C. Debnath, S. A. Hussain & D. Bhattacharjee (2016) Formation of J-aggregates in Langmuir-Blodgett films: Effect of stearic acid and nano clay platelets, Molecular Crystals and Liquid Crystals, 638:1, 44-59, DOI: 10.1080/15421406.2016.1221944

To link to this article: http://dx.doi.org/10.1080/15421406.2016.1221944

Published online: 14 Nov 2016.

Submit your article to this journal

Article views: 13

View related articles

View Crossmark data

Full Terms & Conditions of access and use can be found at
http://www.tandfonline.com/action/journalInformation?journalCode=gmcl20

Download by: [College of Business Education] **Date:** 22 December 2016, At: 12:28

MOLECULAR CRYSTALS AND LIQUID CRYSTALS
2016, VOL. 638, 44–59
http://dx.doi.org/10.1080/15421406.2016.1221944

Taylor & Francis
Taylor & Francis Group

Formation of J-aggregates in Langmuir-Blodgett films: Effect of stearic acid and nano clay platelets

A. Shil[a], C. Debnath[b], S. A. Hussain[a], and D. Bhattacharjee[a]

[a]Thin Film and Nanoscience Lab, Department of Physics, Tripura University, Suryamaninagar, Tripura, India; [b]Department of Physics, MBB College, Agartala, Tripura, India

ABSTRACT

In the present communication, a water soluble prophyrin derivative, tetra-cationic dye 5, 10, 15, 20-tetrakis (1-methyl-4-pyrindino) porphyrin tetra (p-toluenesulfonate) (abbreviated as TMPyP) has been used to prepare stable Langmuir monolayer at the air–water interface by allowing it to adsorb from the aqueous subphase, into the preformed Langmuir monolayer of anionic stearic acid (SA) and cationic octadecylamine (ODA). Anionic nano clay platelets Laponite acted as mediator to initiate adsorption of cationic TMPyP into the cationic ODA monolayer. Surface pressure versus area per molecule (π-A) isotherm studies of SA-TMPyP complex monolayer gave valuable information about the TMPyP molecular area. Organizations of TMPyP molecules were greatly affected in the two different kinds of anionic and cationic matrices. Adsorption led to the flattening of TMPyP molecules in both the matrices. The organization of TMPyP tagged nano clay platelets in preferred direction led to the development of J-band resulting due to the formation J-aggregates in the Langmuir-Blodgett (LB) films. This has been confirmed by UV-vis absorption spectroscopic studies.

KEYWORDS

AFM; isotherm studies; j-aggregates; langmuir-blodgett films; molecular area

1. Introduction

Aggregation of dye in ultra-thin films have attracted considerable interest in recent time owning to their potential applications in various technological fields namely in nonlinear optics, optical memory, organic solar cell, gas sensors, molecular electronics and laser technologies, etc. [1–6]. Nature and organizations of molecular aggregates can be controlled precisely by changing various film forming parameters during the process of preparation of films. Langmuir-Blodgett (LB) film deposition technique is unique in this respect because molecular organizations can be controlled precisely even in monolayer. LB technique is useful for fabrication of nano scale aggregates in ultra-thin films and the aggregation pattern can be precisely controlled by this technique [7]. Different kinds of molecular aggregates are formed in ultra-thin films depending on the molecular organizations. Red shifted sharp absorption band with respect to the monomer is generally referred to as J-band formed due to J-types molecular aggregates. H-aggregates result in the blue shifted absorption band with respect to the monomer.

CONTACT D. Bhattacharjee debu_bhat@hotmail.com Thin Film and Nanoscience Lab, Department of Physics, Tripura University, Suryamaninagar, Tripura, India.
Color versions of one or more of the figures in the article can be found online at www.tandfonline.com/gmcl.
© 2016 Taylor & Francis Group, LLC

J-aggregates in ultra-thin films have found their important applications in spectral sensitization, optical storage, large optical nonlinearities, etc. [8–10]. The first and second order optical hyperpolarizibility is found in J-aggregation which allows second and third harmonic generations [11].

Owing to their high optical nonlinearity arising due to their extended π-conjugated structure [12], porphyrins become promising candidates for nonlinear photonic devices [13,14]. Their rigid planer geometry, high stability, intense electronic absorption band, and small HOMO-LOMO energy gap make porphyrins an amazing candidate for synthetic building blocks for functional nanomaterials. Other applications of porphyrins include gas sensors [4], molecular electronics [5], and solar cells [15].

Free base and metallo-porphyrins are mostly water soluble. They are found to be the most investigating materials due to their crucial roles governing many biological processes such as oxygen transport by hemoglobin [16]. In potential biological applications, porphyrins are mainly used as therapeutic drugs [17] for detection of cancer and also used as photosensitizers in photodynamic therapy of cancer [18]. Recently porphyrins have become a promising candidate for the imaging of tumor [19], treatment of retinal and sub retinal edema [20], nonmalignant conditions such viral and bacterial infections [21]. The structure and orientation of the porphyrin rings in biological systems is important for performing functions such as light-induced charge separation or energy transformation [22]. In this regard, the monolayer formed at the air–water interface and the transferred films onto solid substrates by LB technique are of utmost important to mimic biological systems for investigating the nature of the interactions between porphyrins and others molecules.

Porphyrins form J-aggregates under certain conditions due to hydrophobic π–π stacking and the electrostatic interactions between the anionic and cationic groups. In aqueous solution, molecular aggregation of porphyrins can be tuned depending on porphyrin structure, concentration, pH, ionic strength, counter ions in inorganic salts in the aqueous medium [23–27]. Several other factors namely micelles, ionic liquid, nucleic acid, proteins, nanotubes can influence porphyrin aggregation behavior [28–32].

Aggregation of porphyrins in ultrathin films has been reported by several authors. Water soluble anionic porphyrin TSPP formed aggregates in ultrathin films [33]. Amphiphilic porphyrins formed aggregates in LB film [34]. LB films of porphyrins have been used as gas sensors [35].

Amphiphilic molecules are ideal for LB film preparation [36,37]. In some cases water insoluble nonamphiphilic materials were also observed to formed LB film when they were mixed with building matrices [38]. Water soluble material was also used for the preparation of LB films [39,40]. In such cases, suitable ionic (cationic or anionic) water soluble materials, dissolved in the aqueous subphase of the Langmuir trough are allowed to be adsorbed onto a preformed template Langmuir monolayer of oppositely charged amphiphiles. Due to electrostatic interactions, the water soluble ionic materials are adsorbed into the oppositely charged preformed Langmuir monolayer. Thus a complex/hybrid stable Langmuir monolayer is formed at the air–water interface. Depending on the process of adsorption, organization and orientation of the molecules may change. Surface pressure versus area per molecular isotherms study at the air–water interface may give useful information in this respect.

In the present communication detailed investigations have been carried out to study the nature of organization of a water soluble tetra-cationic porphyrin namely 5, 10, 15, 20-tetrakis (1-methyl-4-pyrindino) porphyrin tetra (p-toluenesulfonate) (abbreviated as TMPyP) molecules in the complex/hybrid Langmuir monolayer as well as also in the complex/hybrid LB films. A comparison between two different types of films has been investigated.

In the first case tetra-cationic TMPyP molecules were adsorbed into the preformed anionic stearic acid (SA) Langmuir monolayer where SA-TMPyP complex molecules were formed. In the second case cationic octadecylamine (ODA) monolayer was used as a template monolayer and the cationic TMPyP molecules were adsorbed into the cationic ODA monolayer via anionic nano clay platelets. In this case, TMPyP molecules were first adsorbed onto the clay platelets via electrostatic interactions and subsequently TMPyP tagged clay platelets were further adsorbed into the preformed cationic ODA monolayer by electrostatic interactions to form organic–inorganic hybrid nano composites. Thus ODA-clay-TMPyP hybrid monolayer was formed at the air–water interface. A detailed investigation has been carried out to study the nature of organization of TMPyP molecules in two different types of films.

2. Experimental section

2.1. Chemicals

Water soluble tetra-cationic dye 5, 10, 15, 20-tetrakis (1-methyl-4-pyrindino) porphyrin tetra (p-toluenesulfonate) (TMPyP) (MW = 1363.6), [purity 99%], SA [purity 99%], and octadecylamine (ODA) [purity 99%] were purchased from Aldrich Chemical Co. and used as received. The clay mineral Laponite used in this study was obtained from the source clays repository of the clay minerals society.

2.2. Instruments

Surface pressure versus area per molecule (π–A) isotherm measurements and LB films preparation were done by a commercially available LB film deposition instrument (Apex-2006C). Ultra pure Milli-Q water (Electrical resistivity 18.2 MΩ-cm) was used as the subphase of the Langmuir trough and was also used to prepare aqueous clay dispersion. Different concentrations of clay dispersions were stirred for 24 hours and then sonicated for 30 minutes prior to use. The temperature was maintained at 24°C throughout the experiment. UV-vis absorption spectrometer (lambda 25, Perkin Elmer) was used to record the UV-vis absorption spectra. For spectroscopic characterizations, thoroughly cleaned quartz substrates were used for LB films preparation. Atomic Force Microscopic (AFM) image of ODA-clay-TMPyP hybrid LB monolayer was taken in air with a commercial AFM system (Bruker Innova). Experiment was performed at room temperature (24 °C). Relative humidity was kept under 60% (non-condensing). First of all, the film was deposited on fresh silicon wafer and then AFM image was taken in ambient air. The AFM image presented here was obtained in intermittent contact (tapping mode). Typical scan area was $2 \times 2\ \mu m^2$.

2.3. Methods

Stock solutions of SA and ODA were prepared by dissolving them in spectroscopic grade chloroform (SRL). The concentration of stock solutions of both SA and ODA was 0.5 mg/ml. Stock solution of TMPyP was made by dissolving it into ultra pure Milli-Q water (10^{-4} M). Same water was used as the subphase in the Langmuir trough for LB film preparation. Aqueous Clay dispersion at different concentrations of Clay (20–80 PPM) were prepared in the ultra pure Milli-Q water and stirred for 24 hours and then sonicated 30 minutes prior to use.

For the preparation of SA-TMPyP complex Langmuir monolayer, first of all required volume (250 and 1000 μL) of TMPyP aqueous solution was dissolved in the aqueous subphase

of the Langmuir trough. Then 60 μL of dilute chloroform solution of SA was spread on the subphase of the Langmuir trough by using a microsyringe. After certain time when the chloroform evaporates only SA molecules lie on the surface of the aqueous subphase of the Langmuir trough. Being anionic SA molecules interact with the cationic TMPyP molecules in the aqueous subphase. As a result TMPyP molecules were adsorbed into the template SA monolayer at the air–water interface and SA-TMPyP complex molecules were formed. Thus a complex Langmuir monolayer was formed at the air–water interface. After waiting for sufficient time to complete the reaction, the monolayer was compressed slowly to obtain the surface pressure versus area per molecule (π–A) isotherm. The complex monolayer was also transferred onto solid substrates to form mono- and multilayered LB films.

Surface pressure versus area per molecule (π–A) isotherm of pure SA monolayer was obtained by spreading 60 μL chloroform solution of SA by a micro syringe on the pure aqueous subphase of the Langmuir trough and the procedure adopted was same as discussed previously with only exception is that there was no dissolved TMPyP molecule in the subphase.

Being cationic, TMPyP molecules could not be directly adsorbed into the template cationic ODA monolayer at the air–water interface. In this case anionic nano clay platelets Laponite acted as mediator to incorporate cationic TMPyP molecules into the ODA monolayer. In such case TMPyP molecules first got adsorbed onto the surface of the anionic clay platelets by electrostatic interactions, subsequently TMPyP tagged nano clay platelets got adsorbed into the cationic ODA monolayer by electrostatic interactions.

Therefore for the preparation of ODA-clay-TMPyP hybrid monolayer at the air–water interface, first of all 250 μL of TMPyP aqueous solution (10^{-4} M) was mixed with the 350 ml aqueous clay dispersion in the Langmuir trough. The clay concentration was 20 PPM for isotherm study and it varied from 20 to 80 PPM for LB film deposition.

After waiting for 30 minutes, 60 μL chloroform solution of ODA was spread onto the subphase of the Langmuir trough by a micro syringe. Adsorption of TMPyP tagged clay platelets onto the ODA monolayer was started immediately. After waiting for one hour to complete the adsorption process Isotherm was recorded.

For the preparation of ODA-clay-TMPyP hybrid LB film, same procedure was followed and after completion of the adsorption process the hybrid monolayer was transferred onto the solid substrate at a surface pressure 20 mN/m and at the speed of 5 mm/min to get mono- and multi- layered LB film.

3. Results and discussion

3.1. Molecular structure and area of TMPyP molecule

Molecular structure of TMPyP is shown in Fig. 1(a). The inter-cationic charge distance between meso-substituent is 1.1 nm as shown in Fig. 1(b) [41]. In aqueous solution, the four meso-substituents are oriented out of plane with respect to the base as shown schematically in Fig. 1(c). In the Langmuir trough when TMPyP molecules interacted electrostatically with the anionic SA molecules in the preformed Langmuir monolayer, four SA molecules were tagged at the four meso-substituents of one TMPyP molecule and thus the meso-substituents might be oriented in plane with respect to the base. This is shown schematically in Fig. 1(d). Considering SA-TMPyP complex molecule as a flattened square, the molecular area should be of the order of 1.21 nm^2. Any deviation from this flatness may result in the decrease of the molecular area. From the surface pressure vs area per molecular isotherm studies we may get an idea about the molecular area of this SA-TMPyP complex molecule.

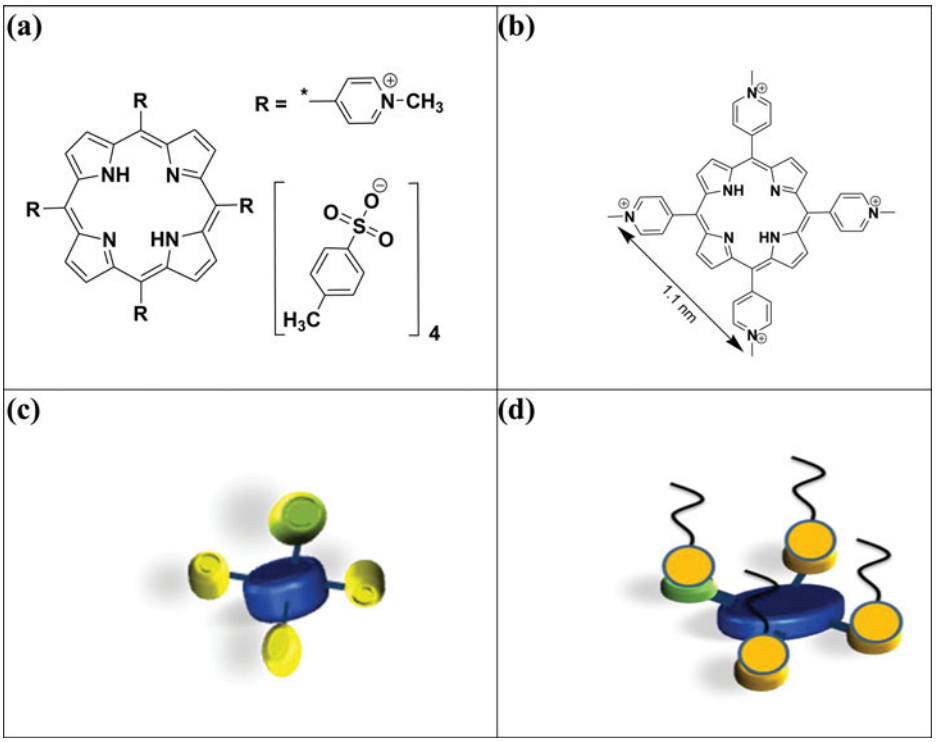

Figure 1. (a) Molecular structure of TMPyP, (b) distance between two meso groups of TMPyP molecule, (c) schemetic representation of one TMPyP molecule in aqueous solution, (d) schematic representation of one SA-TMPyP complex molecule.

3.2. Surface pressure versus area per molecule isotherms studies

3.2.1. Adsorption of water soluble tetra-cationic porphyrin TMPyP into the preformed Langmuir monolayer of anionic SA

Water soluble tetra-cationic dye TMPyP molecules were adsorbed in the preformed anionic SA monolayer at the air–water interface by electrostatics interactions. This resulted in the formation of SA-TMPyP complex monolayer. Figure 2(a) shows the surface pressure versus area per molecule isotherms (π–A) of SA on (I) pure aqueous subphase, (II) 250 μl aqueous solution of TMPyP mixed aqueous subphase and (III) 1000 μL aqueous solution of TMPyP mixed aqueous subphase of the Langmuir trough. The spreading amount of chloroform solution of SA (concentration 0.5 mg mL^{-1}) was remained fixed at 60 μL in all the cases and the concentration of TMPyP aqueous solution was kept fixed at 10^{-4}M. The isotherms were recorded after waiting for 30 minutes to complete the interactions. All the isotherms were the average of three independent sets. Isotherms II and III show the complex SA-TMPyP monolayer isotherms for 250 μl and 1000 μl TMPyP aqueous solution mixed aqueous subphase of the Langmuir trough.

As shown in Fig. 2(a), SA isotherm on pure aqueous subphase is a smoothly rising curve with initial lift-off area 0.276 nm^2 and at a surface pressure of 25 mN m^{-1}, the area per molecule becomes 0.21 nm^2 and this is the limiting area of SA. These values as well as the shape of the isotherm are in good agreement with the reported results in the literature [42,43].

The isotherms of SA-TMPyP complex monolayer in both the cases showed higher lift-off area than that of pure SA monolayer which is the clear evidence of the adsorption of

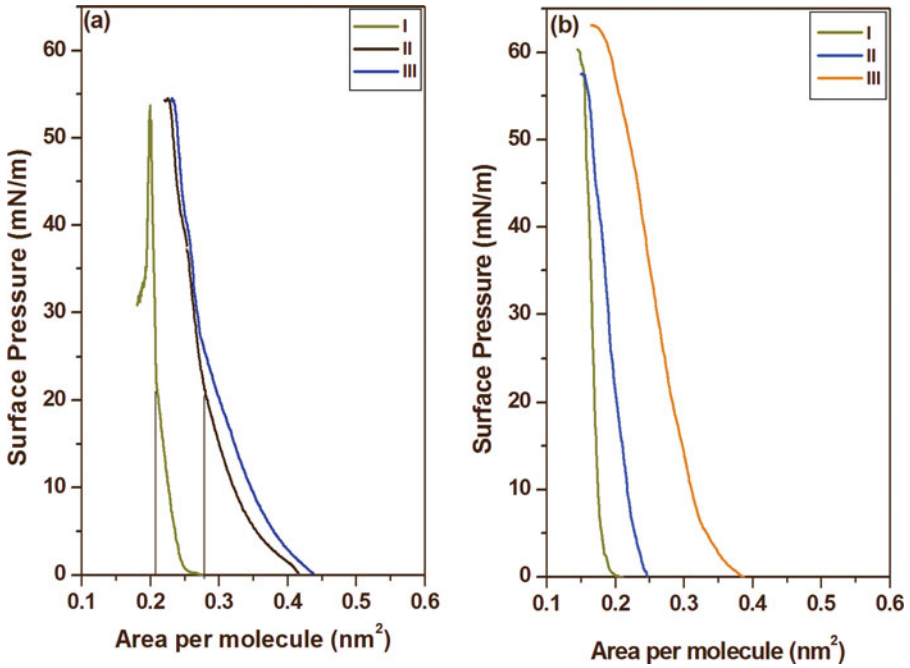

Figure 2. (a) Surface pressure versus area per molecule isotherms of (I) SA on pure aqueous subphase, (II) SA on 250 μL TMPyP mixed aqueous subphase, (III) SA on 1000 μL TMPyP mixed aqueous subphase; (b) Surface pressure versus area per molecule isotherms of (I) ODA on pure aqueous subphase, (II) ODA-clay hybrid monolayer, (III) ODA-clay-TMPyP hybrid monolayer.

tetra-cationic TMPyP molecules into the anionic head groups of SA molecules. As TMPyP molecules were attached to the hydrophilic part of the SA molecules, the molecular area of the complex molecule became greater than that of pure SA molecule. This resulted in the increased molecular area of the complex molecule at the air–water interface. Another interesting point to note is that in both the isotherms of complex monolayer, the initial lift off area remained same. Both the isotherms also have the same limiting area of 0.28 nm^2. Moreover both the isotherms almost coincided. This indicates that 250 μL solution of TMPyP was sufficient to compensate the charges of all the SA molecules at the air–water interface. No more SA molecules were left free to interact with the excess TMPyP molecules in the 1000 μL solution of TMPyP in the aqueous subphase of the Langmuir trough.

The most interesting point to note is that in the SA-TMPyP complex molecule, four meso-substituent of a TMPyP molecule are electrostatically attached to the anionic parts of the four SA molecules. Since TMPyP molecules are water soluble, the isotherm characteristic curve shows the area per molecule with respect to the number of pure SA molecules. Even the isotherm of complex monolayer is accounted with respect to the number of SA molecules introduced initially at the air–water interface. The increase in the limiting area per molecule of complex monolayer indicates an increase in area surrounding one SA molecule at the air–water interface. As shown in the Fig. 1(d), one SA-TMPyP complex molecule was formed when four SA molecules were attached to the four meso-substituent of one TMPyP molecule. Thus the limiting SA area per molecule in the complex monolayer multiplied by four gives the area per molecule of one SA-TMPyP complex molecule. That is also we may get an idea about the TMPyP molecular area. The limiting area per molecule as calculated from the isotherm of complex monolayer was 0.28 nm^2, as shown in Fig. 2(a). Therefore, the TMPyP molecular

area should be about $0.28 \times 4 = 1.12$ nm^2. It is little less than the TMPyP molecular area of 1.21 nm^2 as discussed in the previous section. Therefore it may be concluded that when SA-TMPyP complex molecules were formed at the air–water interface, the degree of flatness of TMPyP molecules was mostly achieved although not completely flattened.

The flattening of TMPyP molecule upon adsorption onto SA monolayer has been further confirmed by UV-vis absorption spectroscopic studies as discussed in later section.

3.2.2. Adsorption of clay tagged TMPyP molecules into cationic octadecylamine (ODA) monolayer

In order to investigate the effect of nano clay platelets on the organization of TMPyP molecules in the LB films, cationic amphiphiles octadecylamine (ODA) was chosen to prepare the template Langmuir monolayer. Being cationic ODA molecules do not interact electrostatically with the cationic TMPyP molecules. For TMPyP molecules to be adsorbed into the ODA template monolayer, anionic nano clay platelets Laponite was chosen as a mediator. In the clay dispersed aqueous subphase of the Langmuir trough, 250 μL aqueous solution of TMPyP (10^{-4}M) was mixed. Being cationic, TMPyP molecules got adsorbed on the anionic sites of the clay platelets. Then ODA monolayer was prepared on the subphase containing aqueous dispersion of TMPyP tagged clay platelets. Due to electrostatic interactions, TMPyP tagged nano clay platelets were further adsorbed into the cationic ODA monolayer. As a result, ODA-clay-TMPyP hybrid Langmuir monolayer was formed at the air–water interface. Formation of this hybrid monolayer can be confirmed from the surface pressure versus area per molecule isotherm studies of this hybrid monolayer. The term hybrid is used here in the sense that in this case organic–inorganic composites were formed. The organic-inorganic composite monolayer thus formed at the air–water interface is called hybrid monolayer.

Figure 2(b) shows the (I) pure ODA isotherm, (II) ODA-clay hybrid monolayer isotherm, (III) ODA-clay-TMPyP hybrid monolayer isotherm.

ODA isotherm on pure aqueous subphase shows a steep rising indicating the highly condensed and low compressible characteristics of ODA monolayer and same as reported elsewhere [44]. ODA-clay hybrid monolayer isotherm was measured on the clay dispersed aqueous subphase at ambient condition with freshly prepared deionized distilled water. From the figure it is observed that ODA-clay hybrid monolayer isotherm has higher area per molecule than that of pure ODA isotherm which is the clear evidence of the adsorption of anionic clay platelets into the cationic template ODA monolayer.

Graph (III) in Fig. 2(b) shows the isotherm of ODA-clay-TMPyP hybrid monolayer with 250 μL aqueous solution of TMPyP. From the graph it is observed that the area per molecule of ODA-clay-TMPyP hybrid monolayer is higher than that of even ODA-clay hybrid monolayer. As clay surface has large number of anionic sites, initially cationic TMPyP molecules got adsorbed on the surface of clay platelets and subsequently TMPyP tagged nano clay platelets were further adsorbed into the cationic ODA monolayer. The organization of TMPyP molecules on the clay platelets led to the increase of area per molecule of the hybrid monolayer at the air–water interface. This has been explained schematically in Figs. 3(a) and (b).

In Fig. 3(a), schematic representation of ODA-clay hybrid molecule is shown. Nano clay platelet Laponite has a plate like structure having a large number of anionic sites on the surface. When it was adsorbed on the template cationic ODA monolayer at the air–water interface from the aqueous clay dispersion, cationic head group of the ODA molecules interacted electrostatically with the anionic sites of the clay platelet and thus the ODA molecules were tagged on the clay surface. However it is not possible to confirm quantitatively the exact

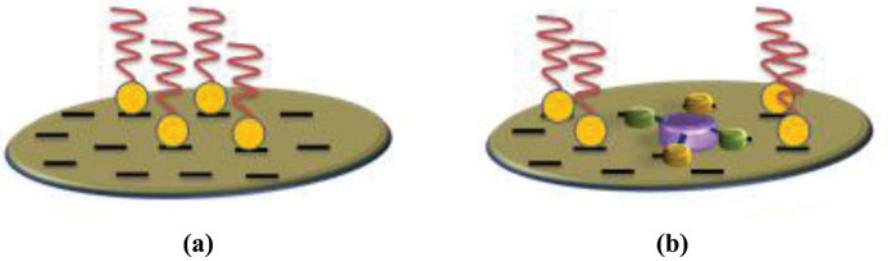

Figure 3. (a) Schematic representation of ODA-clay hybrid molecule, (b) Schematic representation of ODA-clay-TMPyP hybrid molecule.

number of ODA molecules adsorbed on the clay surface since there is large number of anionic sites present on the clay platelets. But since upon adsorption on the clay platelets, the effective area surrounding one ODA molecules was increased, it resulted in the overall increase of area per molecule of the ODA-clay hybrid monolayer.

In the TMPyP mixed aqueous clay dispersion, the cationic charges present at the four meso-substituent of a TMPyP molecule interacted with the four neighboring anionic sites of a nano clay platelet, got adsorbed and became flattened on the clay platelet. Subsequently, cationic sites of the ODA molecules from the template ODA monolayer further interacted with the few more extra anionic sites left on the clay platelets and formed ODA-clay-TMPyP hybrid molecules. Thus ODA-clay-TMPyP hybrid monolayer is formed at the air–water interface. This is shown schematically in Fig. 3(b). As a result the effective area per molecule surrounding one ODA molecule was sufficiently increased. Therefore the area per molecule of this hybrid monolayer was increased as evidenced from the Isotherm characteristics of the ODA-clay-TMPyP hybrid monolayer.

3.3. UV-vis absorption spectroscopy

3.3.1. SA-TMPyP complex LB film

UV-vis absorption spectroscopic studies give valuable information about the nature of molecular organizations in the LB film. Once the complex monolayer was formed at the air–water interface, the monolayer was transferred onto solid substrate by Y-type deposition technique to form mono- and multilayer LB films. For UV-vis absorption spectroscopic studies, quartz substrates were used for LB film deposition.

The UV-vis absorption spectrum of aqueous solution of TMPyP consists of strong transition to the second excited state (S_0-S_2) known as Soret band or B-band and a weak transition to the first excited state (S_0–S_1) termed as Q-band. Both B and Q bands arise from π–π^* transition and can be explained by the four orbital model of Gouterman [45]. The Soret band position is highly sensitive to microenvironment [46,47].

Figure 4(a) shows the UV-vis absorption spectra of (I) aqueous solution of TMPyP (2×10^{-4} M) (II) thin cast microcrystal film of TMPyP and (III) monolayer SA-TMPyP complex LB film. TMPyP aqueous solution shows two distinct absorption bands [48], one is the high energy soret band with peak at 421 nm. The other consists of a number of weak bands in the 500–650 nm regions called Q-bands. A similar spectral profile of the Soret band was reported by Vlekova et al. [49].

A comparison of UV-vis absorption spectra of TMPyP thin cast microcrystal film and monolayer SA-TMPyP complex LB film has been made in order to get an idea about the

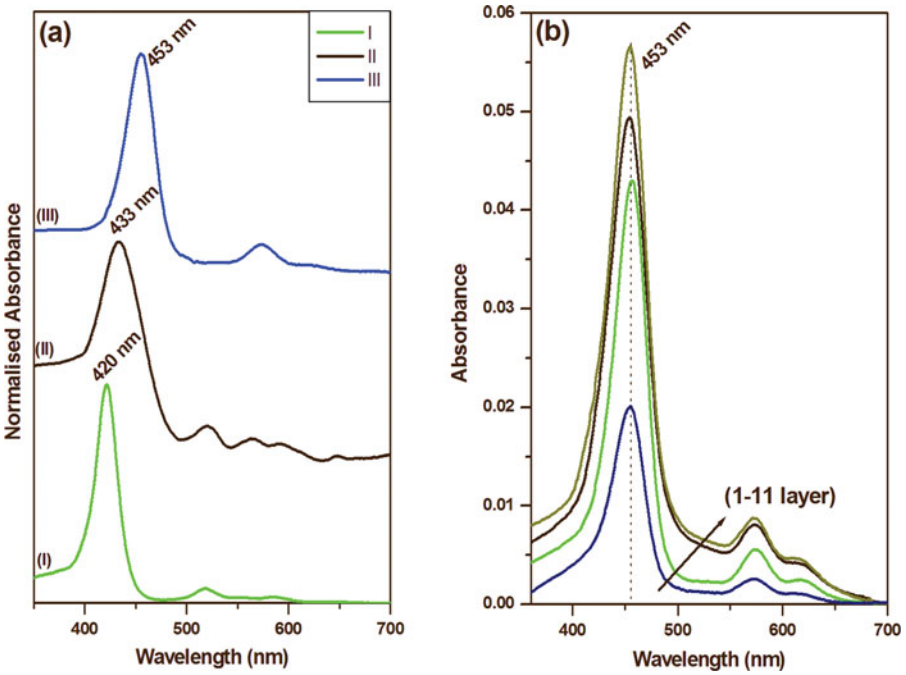

Figure 4. (a) Normalized UV-vis absorption spectra of (I) aqueous solution of TMPyP [10^{-5}M], (II) thin cast microcrystal film of TMPyP and (III) SA-TMPyP complex monolayer LB film; (b) UV-vis absorption spectra of different layered SA-TMPyP complex LB film.

nature of molecular organization in both types of film. Better control on molecular organization can be achieved in LB film unlike that of thin cast microcrystal (MC) film. However in some cases self-assembly results in the molecular organization even in thin cast MC film. These may sometimes lead to the formation of aggregation.

Thin cast MC absorption spectrum shows red shifted Soret peak at 433 nm with a broadened spectral profile. Q-bands lie almost in the same positions. In monolayer LB film there is a large red shifting of Soret peak which is at 453 nm. It is a 20 nm red shifting in comparison to the microcrystal film and more than 30 nm red shifting than that of aqueous solution. Moreover, the Soret band is also broadened. The large red shifting of the Soret band in the LB film cannot be explained readily. It may be mentioned in this context that Takagi et al. reported the red shifting of about 30 nm in the peak position of TMPyP molecules upon adsorption onto nano clay platelets in aqueous dispersion [50]. This has been explained as due to the flattening of the meso-substituent of TMPyP molecules with respect to the porphyrin ring in the process of adsorption on the charged clay substrate. The spectral shift depends on several factors. First, the molecular flattening extends the π-conjugation of the porphyrin molecule. Second, the resonance electron-withdrawing effect of meso-substituent methylpyridinium groups is enhanced, suggesting that both HOMO and LUMO are stabilized, especially for LUMO. Thus, when the meso-substituent rotate towards the coplanar conformation with respect to the porphyrin ring (i.e., flattening), the absorption spectrum is shifted to the longer wavelength, which corresponds to the decrease of the HOMO–LUMO gap [51].

Therefore, it may be concluded that the large red shifting of the Soret peak in the monolayer SA-TMPyP complex LB film may be due to the flattening of the meso-substituent of TMPyP molecules with respect to the porphyrin ring, when electrostatically attached to the anionic

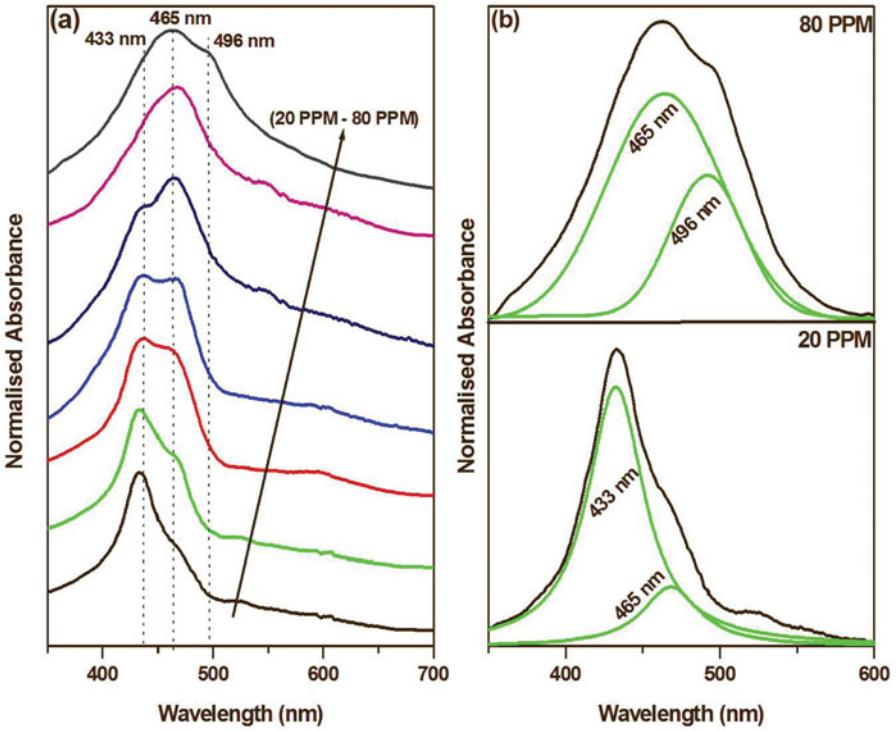

Figure 5. (a) Normalized UV-vis absorption spectra of monolayer LB films of ODA-clay-TMPyP hybrid film at different clay concentration; (b) deconvoluted normalized UV-vis absorption spectra of monolayer LB film of ODA-clay-TMPyP hybrid film at 80 PPM and 20 PPM clay concentration.

parts of the SA molecules. This is schematically shown in Fig. 1(d). Isotherm characteristics study of the complex monolayer discussed in the previous section also supported this thesis.

Figure 4(b) shows the UV-vis absorption spectra of different layered SA-TMPyP complex LB film. Absorbance intensity increased with increasing layer number but no change in peak position of the Soret band was observed. This also supported our thesis that the red shifting of Soret peak was due to the flattening of the porphyrin moieties upon adsorption onto SA monolayer.

3.3.2. ODA-clay-TMPyP hybrid LB film

Figure 5(a) shows the UV-vis absorption spectra of ODA-clay-TMPyP hybrid monolayer LB films prepared from the different Langmuir monolayer on aqueous clay dispersion at different clay PPM concentration. All the films were lifted at 20 mN m^{-1} surface pressure. When the monolayer film was prepared at 20 PPM clay concentration, Soret band was observed with an intense peak at 433 nm along with a weak hump at 465 nm. The UV-vis absorption spectra of the films prepared with increasing clay PPM concentration in the aqueous clay dispersion of the Langmuir trough showed interesting results. The Soret peak at 433 nm gradually reduced in intensity and the 465 nm peak became intense with increasing clay PPM concentration. At higher clay concentration, the 433 nm peak intensity almost reduced to zero. At 80 PPM clay concentration, along with intense 465 nm peak, a weak hump at 496 nm was also observed.

At lower clay concentration of 20 PPM the marked similarities of Soret band along with Soret peak position of the LB film and thin cast MC film [shown in Fig. 2(a)] have been

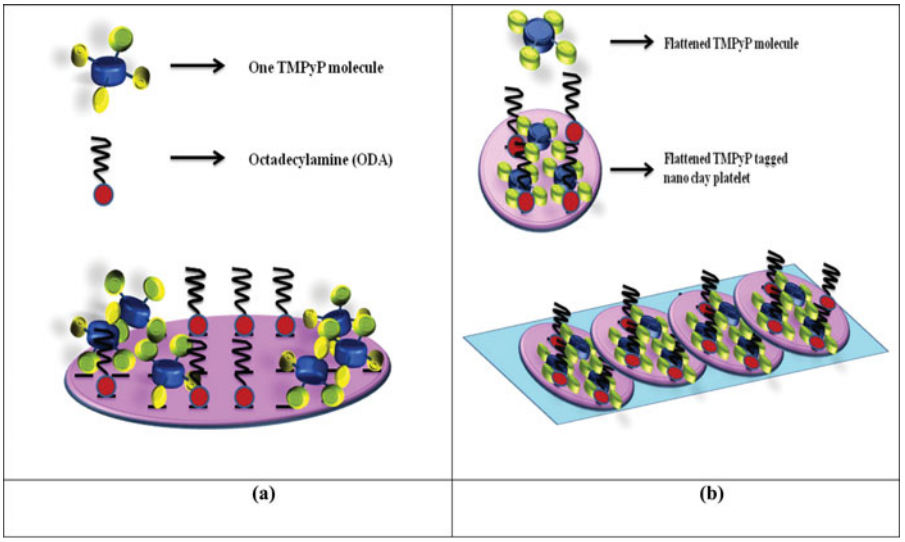

Figure 6. (a) Schematic representation of the association of TMPyP molecules on a single clay platelet at 20 PPM clay concentration. (b) Schematic representation of ODA-clay-TMPyP hybrid LB film at 80 PPM clay concentration where clay platelets are oriented in a preferred direction.

observed. It can be definitely concluded that microcrystalline aggregates were formed in the LB film at such small PPM of clay concentration.

It may be worthwhile to mention in this context that at such low PPM clay concentration, due to the nonavailability of sufficient number of nano clay platelets not all the meso-substituent of all the TMPyP molecules got adsorbed on the clay platelets. Might be one or two meso-substituent of one TMPyP molecule was attached onto the nano clay platelets. In this way a large number of TMPyP molecules might be attached onto single nano clay platelet. This may be termed as weak adsorption. The TMPyP molecules were forced to come closer on the nano clay platelets and became immobilized when the clay platelets were adsorbed into the ODA monolayer and formed hybrid LB film on the solid substrate. Thus TMPyP microcrystalline aggregates were formed on the clay platelets in the LB film. Nonavailability of sufficient number of clay platelets led to the formation of microcrystalline aggregates of TMPyP molecules in the LB films. This is shown schematically in Fig. 6(a).

With increasing clay concentration, all the four meso-substituent of several TMPyP molecules were electrostatically attached to the clay platelets and became flattened. The flattening of TMPyP molecules resulted in the development of 465 nm peak. The origin of this peak has been explained in previous section and also discussed by Takagi et al. [49].

The most interesting observation is that for the film prepared at 80 PPM clay concentration, a weak hump was developed at 496 nm along with an intense 465 nm peak. 496 nm hump was not observed at lower clay concentration. The origin of this longer wavelength 496 nm hump cannot be explained readily. This band cannot be ascribed as due to the flattening of the porphyrin moieties. In this respect several authors reported that the longer wavelength band in the 480–500 nm regions in the UV-vis absorption spectra of porphyrin might be originated as due to the formation of J-aggregates under different conditions. Belfield et al. [50] reported that a functional polymer could be templated to construct a supramolecular assembly of porphyrin based dye to facilitate J-aggregation and referred the origin of J-band at 490 nm as due to the self-assembly of obliquely stacked hydrophobic porphyrin rings. Periasamy et al. reported the formation of J-aggregation of anionic porphyrin derivatives TPPS

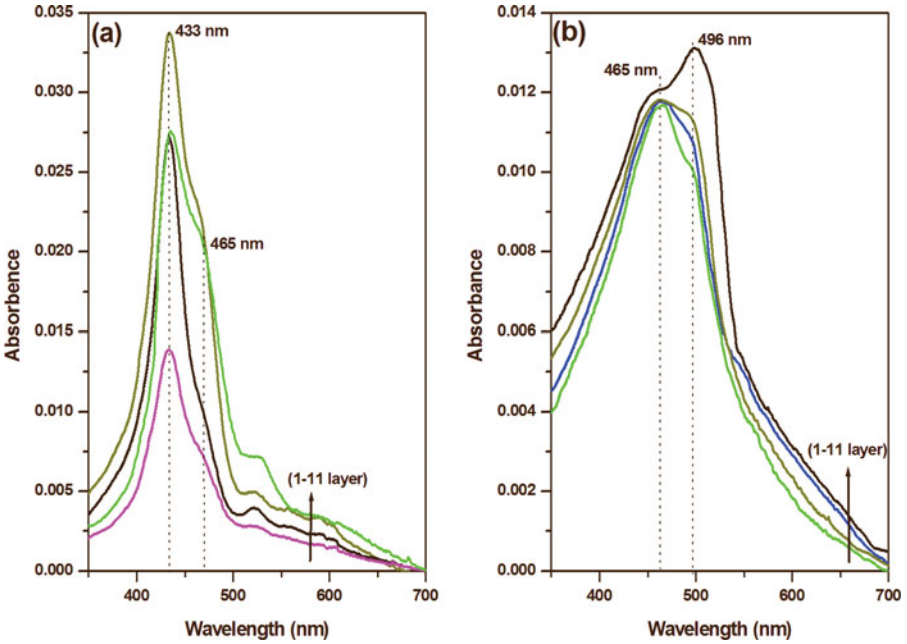

Figure 7. (a) Different layered LB film of ODA-clay-TMPyP hybrid film at 20 PPM clay concentration; (b) different layered LB film of ODA-clay-TMPyP hybrid film at 80 PPM clay concentration.

with cationic surfactants in aqueous solution at pH 3.0 [52]. pH induced J-aggregates of TPPS in the micellar core has been investigated by Shi et al. and reported the J-band at 490 nm [53]. The existence of J-aggregation of TSPP in LbL film has been reported by Ruggles et al. and J band was formed at 486 nm [54]. Therefore it is certain that 496 nm band in the monolayer LB film prepared at 80 PPM clay concentration is the J-band arising due to the J-type aggregation.

At higher clay PPM concentration, due to the availability of large number of anionic nano clay platelets, all the four meso-substituent of TMPyP molecules were attached onto the nano clay platelets by electrostatic interactions and thus the molecules became completely flattened. These flattened TMPyP molecules tagged nano clay platelets formed the organo-clay hybrid molecules. These TMPyP tagged nano clay platelets were further associated in the hybrid LB film in a preferred direction to form J-aggregates. Therefore, the longer wavelength band with peak at 496 nm is the J-band arising due to the formation of obliquely stacked clay platelets in the LB film, where the TMPyP molecules have been completely flattened onto the nano clay platelets. Due to the stacking of clay platelets, the flattened TMPyP molecules onto different clay platelets were also obliquely stacked resulting in the formation of J-aggregates. This is shown schematically in Fig. 6(b). It may be mentioned in this context that the characteristic features of J-band is the red shifting with respect to the monomer band as well as also the sharp peak [47,48]. However in the present case due to overlapping of J-band with the high energy band, a broad band was observed.

Figure 5(b) shows the deconvolution of the absorption spectra of monolayer LB film at 80 and 20 PPM clay concentration in the aqueous dispersion of the Langmuir trough. When the LB film is prepared at the lower clay concentration of 20 PPM in the clay dispersion the Soret band is resolved into two Gaussian curve having peaks at 433 and 465 nm. When the LB film is prepared at higher clay concentration of 80 PPM in the aqueous clay dispersion, the Soret band was deconvoluted into two bands one intense band with peak at 465 nm and other weak peak at 496 nm whereas the 433 nm band remained absent.

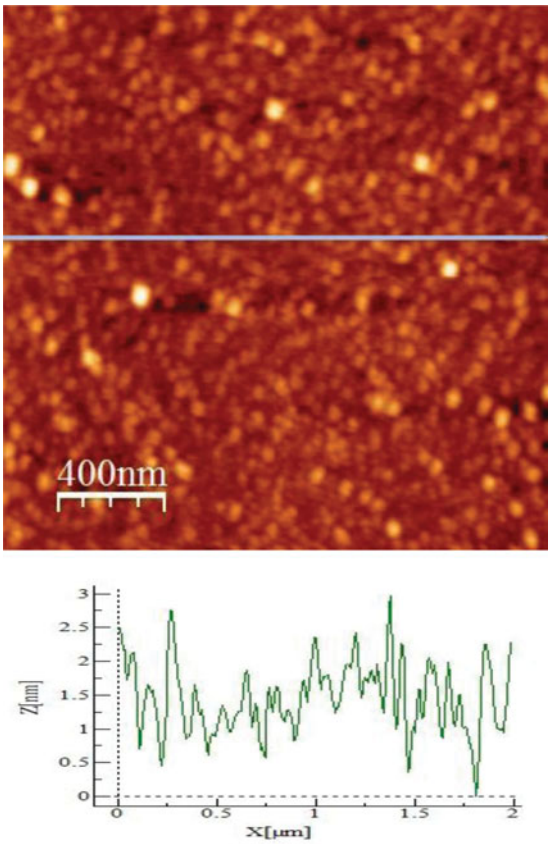

Figure 8. AFM image of monolayer LB film of ODA-clay-TMPyP hybrid film at 80 PPM clay concentration.

It is clearly evident from the deconvolution spectra that at lower clay concentration less number of sample molecules were completely adsorbed followed by complete flattening on clay platelets. Existence of intense 433 nm peak indicates the formation of molecular aggregates at such lower clay concentration.

At higher clay concentration of 80 PPM intense band with peak at 465 nm and absence of 433 nm peak indicate that most of the sample molecules were adsorbed on the clay platelets and consequently became flattened. The sample tagged clay platelets also became oriented in a preferred direction to form J-aggregates. This is the origin of the J-band at 496 nm.

3.3.3. Layer effect

Figure 7 shows the UV-vis absorption spectra of the different layered hybrid LB film of TMPyP-clay hybrid molecules. Figure 7(a) shows the corresponding absorption spectra prepared at lower 20 PPM clay concentration and Fig. 7(b) shows corresponding absorption spectra at higher clay concentration of 80 PPM in the aqueous clay dispersion. For LB films prepared at lower clay concentration, intensity of 433 nm peak was increasing with layer number along with a hump at 465 nm. Relative intensity of the peak position remained almost same. It indicates the formation of microcrystalline domains in the LB film with increasing layer number.

Figure 7(b) shows interesting observation. With increasing layer number 496 nm J-band became prominent and at higher layer number it became intense along with 465 nm band which is originated due to flattening of porphyrin moieties. Intense J-band at 496 nm indicates

the association of large number of sample tagged clay platelets in preferred direction forming J-aggregates.

4. AFM study

Figure 8 shows the AFM image of ODA-clay-TMPyP hybrid monolayer LB film prepared on freshly washed Si wafer. The film was fabricated at clay concentration of 80 PPM on the clay dispersed aqueous subphase of the Langmuir trough. Densely packed disk like nano clay platelets are closely visible in the AFM image. The surface coverage is more than 90%. The clay platelets are overlapped on each other and formed tilled organization. The ODA and TMPyP are not distinguishable since the dimensions of these molecules are beyond the resolution of AFM system. The average thickness of the film is around 2 nm as evidenced from the height profile study. However, the thickness of single clay platelets is (1.1–1.2) nm. Therefore, the average thickness of the film more than 2 nm indicates overlapping and tilted organizations of clay platelets in the monolayer hybrid LB film. As a result flattened TMPyP molecules on nano clay platelets formed preferred organization and developed J-aggregated sites.

5. Conclusion

In conclusion, our results showed that water soluble tetra-cationic dye TMPyP molecules were adsorbed into the preformed anionic SA monolayer by electrostatic interaction and thus a complex SA-TMPyP Langmuir monolayer was formed at the air–water interface. The adsorption led to the almost flattened configuration of TMPyP molecules in the complex monolayer. Surface pressure versus area per molecule (π–A) isotherm studies of this complex monolayer gave valuable information in this regard. The molecular area of TMPyP molecule was calculated from the SA-TMPyP isotherm graph. UV-vis absorption spectroscopic studies of the SA-TMPyP complex LB films also supported the flattened organization of TMPyP molecules in the SA-TMPyP complex LB film. On the other hand, nano clay platelets Laponite acted as mediator in the process of adsorption of cationic TMPyP molecules into the preformed cationic ODA monolayer. In this process cationic TMPyP molecules were first adsorbed on the surface of the anionic nano clay platelets. Subsequently TMPyP tagged nano clay platelets were adsorbed into the preformed cationic ODA monolayer. Thus a hybrid organic-inorganic nano composites namely ODA-clay-TMPyP hybrid molecules were formed and the hybrid monolayer was formed at the air–water interface. UV-vis absorption spectroscopic studies of this hybrid monolayer confirmed that TMPyP molecules became flattened while absorbed on the nano clay platelets. At higher clay PPM concentration, TMPyP tagged nano clay platelets in the LB films organized in a preferred direction to form J-aggregated sites which was confirmed by UV-vis absorption spectroscopic studies.

Acknowledgments

Dr. S. A. Hussain is grateful to DST for financial support through DST Project (Ref. No. MR/2014/000234; dated 17.03.2015). The authors also acknowledge the financial support under FIST Program – 2014 (Ref. SR/FST/PSI-191/2014 dated 21.11.2014). Mr. Chandan Debnath is grateful to UGC-NERO for financial support through UGC project (Ref. No. F.5-378/2014-15/MRP/NERO/2235).

References

[1] Herrere, F., Peropadre, B., Pachon, L.A., Saikin, S.K. & Guzik. (2014). *J. Phys. Chem. Lett.*, *5*, 3708–3715.
[2] Spano, F.C. & Siddiqui, S. (1999). *Chem. Phys. Lett.*, *314*, 481–487.
[3] Borsenberger, P.M. & Weiss, D.S. Photoreceptors for Imaging Systems; Marcel Dekker: New York, 1993.
[4] Han, B.H., Manners, I. & Winnik. M.A. (2005), *Chem. Mater*., *17*, 3160–3171.
[5] Kang, B.K., Aratani, N., Lim, J.K., Kim, D., Osuka, A. & Yoo K.H. (2006). *Mater. Sci. Eng. C.*, *26*, 1023–1027.
[6] Maeda, M. Lasers Dyes; Academic Press: Tokyo, 1984.
[7] Ariga, K., Yamauchi, Y., Mori, T. & Hill, J.P. (2013) *Adv. Mater.*, *25*, 6477–6512.
[8] Kobayashi, T. J-Aggregates; World Scientific: Singapore, 1996.
[9] Clark, J. & Lanzani, G. (2010). *Nat. Photon.*, *4*, 438–446.
[10] Kobayashi, T., Matsumoto, S., Aoyama, T. & Wada, T. (2006). *Thin Solid Films*, *509*, 145–148.
[11] Wang. Y. (1991). *J. Soc. Opt. Am. B.*, *8*, 981–985.
[12] Senge, M.O., Fazekas, M., Notaras, E.G.A., Blau, W.J., Zawadzk, M., Locos, O.B. & Mhuircheartaigh, E.M.N. (2007). *Adv. Mater.*, *19*, 2737–2774.
[13] Singh, C.P., Bindra, K.S., Jain, B. & Oak, S.M. (2005). *Opt. Commun.*, *245*, 407–414.
[14] Xu, Y.F., Liu, Z.B., Zhang, X.L., Wang, Y., Tian, J.G., Huang, Y., Ma, Y.F., Zhang, X.Y. & Chen, Y.S. (2009). *Adv. Mater.*, *21*, 1275–1279.
[15] Martinson, A.B.F., Massari, A.M., Lee, S.J., Gurney, R.W., Splan, K.E., Hupp, J.T. & Nguyen, S.T. (2006). *J. Electrochem. Soc.*, *153*, 527–532.
[16] Kadish, K.M., Smith, K.M. & Guilard, R., The Porphyrin Handbook; Academic Press: San Diego, CA, 2000; Vol. *VI*, Chapters 40—46.
[17] Chen, X., Hui, L., Foster, D.A. & Drain, C.M. (2004). *Biochemistry.*, *43*, 10918–10929.
[18] Sternberg, E.D., Dolphin, D. & Bručkner, C. (1998). *Tetrahedron*, *54*, 4151–4202.
[19] Ethirajan, M., Chen, Y., Joshy, P. & Pandey, R.K. (2011), *Chem. Soc. Rev.*, *40*, 340–362.
[20] Van Lier, J.E., Tian, H., Ali, H., Cauchon, N. & Hassessian, H.M. (2009). *J. Med. Chem.*, *52*, 4107–4110.
[21] Tsuchida, T., Zheng, G., Pandey, R.K., Potter, W.R. & Bellinier, D.A. (1997). *Photochem. Photobiol*, *66*, 224–228.
[22] Pagona, G., Zervaki, G.E., Sandanayaka, A.S.D., Ito, O., Charalambidis, G., Hasobe, T., Coutsolelos, A.G. & Tagmatarchis, N. (2012). *J. Phys. Chem. C.*, *116*, 9439–9449.
[23] Arai, Y. & Segawa, H. (2011). *J. Phys. Chem. B.*, *115*, 7773–7780.
[24] Hollingsworth, J.V., Richard, A.J., Vicente, M.G.H. & Russo, P.S. (2012). *Biomacromolecules*,*13*, 60–72.
[25] Siskova, K., Vlckova, B. & Mojzes, P. (2005). *J. Mol. Struct.*, *744*, 265–272.
[26] Afzal, S., Daoud, W.A. & Langford, S.J. (2013). *ACS Appl. Mater. Interfaces*., *5*, 4753–4759.
[27] Zawadzka, M., Wang, J., Blau, W.J. & Senge, M.O. (2013). *J. Phys. Chem. A.*, *117*, 15–26.
[28] Li, X., Li, D., Zeng, W., Zou, G. & Chen, Z. (2007). *J. Phys. Chem. B.*, *111*, 1502–1506.
[29] Dutta, P., Rai, R. & Panday, S. (2011). *J. Phys. Chem. B.*, *115*, 3578–3587.
[30] Lee, M., Jin, B., Lee, H.M., Jung, M.J. & Kim, S.K. (2008). *J. Bull. Korean Chem. Soc.*, *29*, 1533–1538.
[31] Brunet, C., Antoine, R., Lemoine, J. & Dugourd, P. (2012). *J. Phys. Chem. Lett.*, *3*, 698–703.
[32] Hasobe, T., Fukuzumi, S. & Kamat, P.V. (2005). *J. Am. Chem. Soc.*, *127*, 11884–11885.
[33] Jiang, S. & Liu, M. (2004). *J. Phys. Chem. B.*, *108*, 2880–2884.
[34] Prieto, I., Pedrosa, J.M., Martın-Romero, M.T., Molbius, D. & Camacho, L. (2000). *J. Phys. Chem. B.*, *104*, 9966–9972.
[35] Tepore, A., Serra, A., Arnold, D.P., Manno, D., Micocci, G., Genga A. & Valli L. (2001). *Langmuir*, *17*, 8139–8144.
[36] Ulman, A. An Introduction to Ultrathin Organic Films: From Langmuir—Blodgett Films of Self Assemblies; Academic Press: New York, 1991.
[37] Umemura, Y., Yamagishi, A., Schoonheydt, R., Persoons, A. & Schryver, F.D. (2002). *J. Am. Chem. Soc.*, *124*, 992–997.
[38] Debnath, P., Chakraborty, S., Deb, S., Nath, J., Bhattacharjee, D. & Hussain, S.A. (2015). *J. Phys. Chem. C.*, *119*, 9429–9441.
[39] Takahashi, M., Kobayashi, K. & Takaoka, K. (2000). *Langmuir*. *16*, 6613–6621.

[40] Umemura, Y. & Shinohara, E. (2005). *Langmuir*, *21*, 4520–4525.
[41] Ceklovsky, A., Takagi, S. & Bujdak, J. (2011). *J. Phys. Chem. Solids.*, *360*, 26–30.
[42] Kele, P., Orbulescu, J., Mello, S.V., Mabrouki, M. & Lablanc, R.M. (2001). *Langmuir*, *17*, 7286–7290.
[43] Guo, Z., Jiao, T. & Liu, M. (2007). *Langmuir*, *23*, 1824–1829.
[44] Wang, K.H., Sye, M.J., Chang, C.H. & Lee, Y.L. (2012). *Sens. Actuators, B.*, *164*, 29–36.
[45] Gouterman, M. (1963). *J. Mol. Spectrosc.*, *11*, 108–127.
[46] Goncalves, P.J., Franzen, P.L., Correa, D.S., Almeida, L.M., Takara, M., Ito, A.S., Zílio, S.C. & Borissevitch, I. (2011). *Spectrochim. Acta Part A.*, *79*, 1532–1539.
[47] Fujimura, T., Shimada, T., Hamatani, S., Onodera, S., Sasai, R., Inoue, H. & Takagi, S. (2013). *Langmuir*, *29*, 5060–5065.
[48] Ghosh, A., Mahato, P., Choudhury, S. & Das, A. (2011). *Thin Solid Films*, *519*, 8066–8073.
[49] Siskova, K., Vlckova, B. & Mojzes, P. (2005). *J. Mol. Struct.*, *744*, 265–272.
[50] Ishida, Y., Masui, D., Shimada, T., Tachibana, H., Inoue, H. & Takagi, S. (2012). *J. Phys. Chem. C.*, *116*, 7879–7885.
[51] Biswas, S., Ahn, H.Y., Bondar, M.V. & Belfield, K.D. (2012). *Langmuir*, *28*, 1515–1522.
[52] Maiti, N.C., Mazumdar, S. & Periasamy, N. (1998). *J. Phys. Chem. B.*, *102*, 1528–1538.
[53] Zhao, L., Ma, R., Li, J., Li, Y., An, Y. & Shi, L. (2008). *Biomacromolecules*, *9*, 2601–2608.
[54] Smith, A.R.G., Ruggles, J.L., Yu, A. & Gentle, I.R. (2009). *Langmuir*, *25*, 9873–9878.